trum of the sample of BPT 30 femtomole at a phase angle of 64.3° (direct nulling BaP). We have conducted measurements using samples having various concentrations of BPT and BaP. At equal concentrations of BaP and BPT the phase-resolved detection technique can easily null out either the emission of BPT or that of BaP. The results were similar to those discussed previously in solution measurements (Figs. 4A and 4B). When the concentration of the interferant compound (i.e., BaP) was increased, some overlap still remained, even with phase resolution. However, as shown in Fig. 4B, we were able to clearly observe the emission peak of BPT at 380 nm when in the presence of a 50-fold more concentrated solution of BaP. Note that, without the use of phase-resolved detection, the emission of BPT was completely masked by that of BaP. The results in Fig. 5 illustrate the capability of the PR-FIS device to reveal the spectrum of 30 femtomoles of BPT in the presence of much higher amounts of interfering BaP.

CONCLUSION

Over the last decade, fiber optics have found widespread applications in many areas in the communication industry as well as in spectrochemical analysis. Biosensor technology based on fiber optics is currently at the forefront of analytical instrumentation research. The integration of biological systems and optical detection technology promises to open new horizons in medical, clinical, and environmental monitoring applications. The use of phase-resolved detection adds another factor of selectivity to the multidimensional character of fluorescence spectroscopy. The PR-FIS developed in this work can measure human exposure to trace levels of hazardous environmental chemicals. The device may also prove useful for early detection of cancer by monitoring DNA-adducts in body fluids. Our previous studies have successfully shown that the instrument can detect trace amounts of carcinogenic compounds and their metabolites at femtomole levels, in sub-microliter sample volumes.[4] The device may also find useful applications as a screening tool for toxic and infectious agents in the workplace or in the home, and as a patient-monitoring instrument in clinical applications.

ACKNOWLEDGMENTS

This work was sponsored by the National Institutes of Health under Contract Number GM 34730 and the Office of Health and Environmental Research, U.S. Department of Energy, under Contract Number DE-AC05-84OR21400 with Martin Marietta Energy Systems, Inc. Monoclonal antibody against BPT was provided by Dr. R. M. Santella from Columbia University.

1. J. I. Peterson and G. G. Vurek, Science **224,** 123 (1984).
2. W. R. Seitz, Anal. Chem. **56,** 17A (1984).
3. T. Vo-Dinh, G. D. Griffin, K. R. Ambrose, M. J. Sepaniak, and B. J. Tromberg, "Fiberoptics-Based Immunofluorescence Spectroscopy for Monitoring Exposure to Polynuclear Aromatic Compounds," in *Proceedings of 10th International Symposium on Polycyclic Aromatic Hydrocarbons,* M. Cooke and A. J. Dennis, Eds. (Battelle Press, Columbus, Ohio, 1985), pp. 885–901.
4. T. Vo-Dinh, G. D. Griffin, and K. R. Ambrose, Appl. Spectrosc. **40,** 696 (1986).
5. B. J. Tromberg, M. J. Sepaniak, T. Vo-Dinh, and G. D. Griffin, Anal. Chem. **59,** 1226 (1987).
6. T. Vo-Dinh, B. J. Tromberg, G. D. Griffin, K. R. Ambrose, M. J. Sepaniak, and E. M. Gardenhire, Appl. Spectrosc. **41,** 735 (1987).
7. B. J. Tromberg, J. P. Alarie, M. J. Sepaniak, T. Vo-Dinh, and R. Santella, Anal. Chem. **60,** 1901 (1988).
8. *Chemical Analysis of Polycyclic Aromatic Compounds,* T. Vo-Dinh, Ed. (Wiley, New York, 1989).
9. J. R. Lakowicz, Principles of Fluorescence Spectroscopy (Plenum Press, New York, 1983).
10. L. B. McGown and F. V. Bright, Anal. Chem. **56,** 400A (1984).
11. F. V. Bright, Appl. Spectrosc. **42,** 1531 (1988).
12. R. M. Santella, C. D. Lin, W. L. Cleveland, and I. B. Wenstein, Carcinogenesis **5,** 373 (1984).

Fourier Transform Infrared Photopyroelectric Spectroscopy of Solids: A New Technique

A. MANDELIS,* F. BOROUMAND, H. SOLKA, J. HIGHFIELD, and H. VAN DEN BERGH

Laboratoire de Chimie Technique, Ecole Polytechnique Federale de Lausanne, Lausanne CH-1015, Switzerland

A novel analytical technique, Fourier transform infrared photopyroelectric spectroscopy (FT-IR-P²ES) is demonstrated and applied to spectroscopic investigations of solid materials. The salient features of the technique and its advantages over other conventional FT-IR photothermal methods are discussed. A few selected quantitative applications are presented as examples of the versatility and sensitivity of the new technique.

Index Headings: **Infrared; Instrumentation; Photopyroelectric FT-IR; Photothermal spectroscopy; Spectroscopic techniques.**

Received 24 February 1989; revision received 1 June 1989.

* Author to whom correspondence should be sent. Permanent address: Photoacoustic and Photothermal Sciences Laboratory, Department of Mechanical Engineering, University of Toronto, Toronto M5S 1A4, Canada.

INTRODUCTION

The past decade has witnessed the introduction of, and dramatic increase in, the use of FT-IR photothermal methods.[1] The most significant of such methods have been FT-IR photoacoustic spectroscopy (PAS)[2] and photothermal deflection spectroscopy (PDS).[3] These techniques have proven to be very powerful for use with broad

0003-7028/90/4401-0132$2.00/0

classes of condensed phase samples, especially due to the decreased sample preparation time, in comparison to that required for conventional FT-IR techniques;[1] the greater reproducibility of band intensities in FT-IR-PA spectra, compared to diffuse reflectance spectra;[4] the absence of spectral distortions from PA spectra due to the Christiansen effects;[5] and the photothermal spectroscopic ability to produce spectra of samples difficult or impossible to study by other techniques (e.g., conducting polymers,[6] surface-adsorbed species,[7-9] coals,[10] etc.), among other considerations. In spite of their recent popularity, the photothermal FT-IR techniques suffer from several handicaps: Microphonic FT-IR-PAS is sensitive to photoacoustic cell resonances, which might distort the obtained spectra[11] due to the fact that the scanning arm of the interferometer usually covers a modulation frequency bandwidth which includes such resonances (a few Hz–several kHz). The inherently nonlinear resonant behavior may only be avoided by using PA cells with resonant frequency placed outside the effective bandwidth of the FT-IR interferometer scan[12]—a difficult task, since it is usually accomplished by increasing the scanning mirror velocity and thus shifting the effective bandwidth outside the resonance region, at a great expense of signal-to-noise ratio (SNR) performance. Furthermore, the requirement for the presence of a transducing gas, to carry the acoustic signal to the microphone in FT-IR-PAS detection, limits the sensitivity of this technique; any infrared absorbing gas in the sample cell tends to produce PA signals at least 100 times greater than the PA signals arising from the condensed phase sample.[13] Therefore, this interference may distort or completely bury the desired spectrum. Further complications with respect to microphonic FT-IR-PAS quantitation arise in the case of powdered samples of small particle size compared to the minimum thermal diffusion length. For high-porosity powders, the interparticle gas thermal expansion coefficient has been shown[14] to generate a pressure signal dominating any pressure changes due to heat transfer from the solid phase at low optical absorption coefficients. This effect appears as an "extra absorption" signal, thus altering the absorption peak-to-background ratios significantly[14] in the range below 10^3 cm^{-1}. The essentially instantaneous character of the pressure term also modifies the FT-IR-PAS phase substantially in this absorption coefficient range. Additional obstacles to quantitative analysis of microphonic FT-IR-PAS signals stem from acoustic wave interference within the PA cell with significant components at low frequencies in the range of interferometric scans. This effect causes strong perturbations[15] to the microphonic PA phase and must be taken into consideration in quantitative analysis. Cell window absorptions and reflections, in order to be avoided, require KBr windows,[12] while FT-IR-PAS cell sensitivity to ambient noise and low-frequency room vibrations have forced Royce *et al.*[16] to mount their Bomem DA3 interferometer on air suspension legs (an optical table), which improved the SNR by about a factor of five. In general, however, the nature of microphonic transducers used with FT-IR-PAS makes this technique very susceptible to external noise sources.

FT-IR-PDS has several advantages over the respective PAS techniques, mostly stemming from the ability of the former to operate in an open environment, yielding a signal which does not require acoustic transduction. At high scanning speeds, however, the probe laser beam position detector exhibits microphonic noise which limits the SNR.[17] Furthermore, the PDS signal mechanism requires the presence of a thermal-wave transferring fluid phase above the sample, in which a modulation frequency-dependent exponential damping occurs,[18] thus limiting the use of the technique to low frequencies and/or strongly absorbing specimens.[17] The pointing stability of the probe laser beam appears to be of concern at low signal levels and it requires compensation schemes.[3]

The alternative technique of piezoelectric (PZT) FT-IR-PAS can, in principle, compensate for many disadvantages of the microphonic detection technique, yet quantitative analysis of absorption bands obtained with this method has not been reported. In addition, some discrepancies exist between relative band intensities obtained piezoelectrically and microphonically.[13] It appears that the requirement for bonding samples to the PZT transducer and its sensitivity to electromagnetic noise from the interferometer motor has limited the amount of activity with this method.

In view of the aforementioned difficulties with the dominant FT-IR photothermal methods, in this paper we introduce the FT-IR-P^{2}ES technique and discuss several important aspects where photopyroelectric detection appears to have advantages over the other techniques.

In pyroelectric materials a change in the temperature causes the release of electronic charges, thus changing the charge density and potential at the surface. When the temperature change is due to the absorption, and subsequent thermal conversion, of optical radiation, the resulting voltage change across the material is the photopyroelectric effect. Pyroelectric materials are noncentrosymmetric crystals (e.g., the triglycine sulphate family) or lamelar polymeric amorphous-crystalline thin films (e.g., polyvinylidene fluoride and copolymers). Such materials may be fabricated into detector elements by poling in the presence of strong electric fields, so that the detector will acquire a net dipole moment that is relatively stable at room temperature, and by depositing thin metallic electrodes on the surface, which will carry away the extra charges generated by the (photo)pyroelectric effect when the element is operating as part of an electrical detection circuit.

THEORETICAL FOUNDATIONS

The use of thin pyroelectric polyvinylidene fluoride (PVDF) films as photothermal spectroscopic transducers with synchronous detection has been successfully implemented for some time.[19,20] The photopyroelectric voltage generated across a PVDF film in intimate contact with a flat sample carries information about the optical absorption coefficient of the material under investigation, as well as thermal and geometric information. As a result, the full P^{2}ES response is quite complicated mathematically, even in the simplest case of a one-dimensional model—valid when the exciting optical beam size is large in comparison to the sample thickness.[21] In the special case, however, of an optically opaque and thermally thick

pyroelectric transducer, such as the one used in the present work, considerable simplification of the formalism occurs, and the complex P²E signal may be written in the form shown in Eq. 1 at the bottom of the page (see Ref. 21, eq. 28).

In Eq. 1, a highly opaque P²E detector was assumed, so that

$$\beta_p \gg \sigma_p \tag{2}$$

where $\beta_s(\beta_p)$ is the optical absorption coefficient (cm^{-1}) of the sample (pyroelectric), and is a function of wavelength; p is the PVDF pyroelectric coefficient ($=3 \times 10^{-5}$ C/m^2 K);[22] I_0 is the incident optical irradiance (W/m^2); ϵ_0 is the permittivity of free space ($= 8.854 \times 10^{-12}$ C/Vm), and $k = 12$;[22] η_s is the nonradiative quantum efficiency of the sample, a function of wavelength; k_s is the sample thermal conductivity (W/m K); and $\sigma_s(\sigma_p)$ is the sample (pyroelectric) complex thermal diffusion coefficient

$$\sigma_j \equiv (1 + i)a_j \equiv (1 + i)\left(\frac{\omega_0}{2\alpha_j}\right)^{1/2} [cm^{-1}];$$

$$j = s, p \tag{3}$$

where α_j is the thermal diffusivity of the jth material (cm^2/s), and $\omega_0 = 2\pi f_0$ is the angular light intensity modulation frequency; a_j is defined by Eq. 3 and represents the inverse of the RMS thermal probe depth, μ_j (the thermal diffusion length) at f_0; l_s is the (assumed uniform) sample thickness; b_{mn} is a thermal coupling coefficient between adjacent materials m and n:

$$b_{mn} \equiv \frac{k_m\alpha_m}{k_n\alpha_n};$$

$$m, n = g \text{ (gas)}, s \text{ (sample)}, p \text{ (pyroelectric)} \tag{4}$$

in the geometry of Fig. 1, with the gas layer overlying the sample surface. Finally r_s is an optothermal parameter of the sample defined as:

$$r_s \equiv \frac{\beta_s}{\sigma_s}. \tag{5}$$

It is interesting to note that, as expected from a back-surface detection technique, Teramae and Tanaka[12] obtained an expression similar to Eq. 1 for the microphonic PA signal generated at the rear surface of the sample, which they used for quasi-quantitative interpretation of back-surface FT-IR-PAS spectra of bilayered polyethylene (PE)/poly(ethylene terephthalate) (PET) films. In order to carry out their investigations, these authors had to construct an elaborate PA cell which allowed sealing of the gas chamber with the back surface of the sample itself.

For the present work, there are three special cases of Eq. 1, which are of experimental interest in characterizing the FT-IR-P²E detector and its spectroscopic capabilities with respect to specific classes of samples.

Optically Opaque Sample. This case is associated with the condition

$$\beta_s l_s \gg 1 \geqq \exp(-\beta_s l_s) \approx 0 \tag{6}$$

and is important for characterizing reference (R) blackbody FT-IR spectra. Under condition 6, Eq. 1 becomes

$$V_R(\omega_0) \approx \frac{pI_0}{(k\epsilon_0)k_R\sigma_R\sigma_p(b_{pR} + 1)} \exp(-\sigma_R l_R) \tag{7}$$

where it was assumed that $\eta_R = 1$ and the thermal coupling coefficient $b_{gR} \ll 1$, a condition usually satisfied at gas/solid interfaces.[23] If the thickness of the reference layer, l_R, is very small compared to the thermal diffusion length—as is the case with thin opaque films directly sprayed or deposited on the PVDF surface—then Eq. 7 simplifies to the following expression ($b_{pR} = 1$):

$$V_{R_0}(\omega_0) = \frac{pI_0}{2(k\epsilon_0)k_p\sigma_p{}^2}. \tag{8}$$

We may also derive Eqs. 7 and 8 assuming an infinitesimally thin opaque thermal source on the surface of the sample and allowing $l_R \to 0$ in the model presented by John *et al.*;[24] however, those authors' results (Ref. 24, eq. 5 with $l_p \to \infty$) are linearly dependent on the surface absorption coefficient of the sample, β'_s. This quantity is misleading and is an artifact of their model, not appearing in more realistic treatments of the problem.[21] Complete agreement of the model by John *et al.*[24] with Eqs. 7 and 8 can occur upon our setting $\beta'_s I_0 \to I_0$, which makes the resulting expressions independent of the sample optical absorption coefficient, as is expected in photopyroelectric (and general photothermal) saturation.[21,23]

For adaptation to FT-IR detection, Eq. 7 may be written in terms of the spectral wavenumber $\bar{\nu}$ according to the well-known relationship[25]

$$f_0(\bar{\nu}) = 2\nu\bar{\nu} \tag{9}$$

for a Michelson interferometer, where ν is the mirror velocity (cm/s), $\bar{\nu}$ is in cm^{-1}, and f_0 is the modulation frequency (Hz) of the IR radiation intensity. Separating out frequency-dependent quantities in Eq. 7 yields the complex representation

$$V_R(f_0) = |V_R(\bar{\nu})|\, e^{i\theta_R(\bar{\nu})} \tag{10}$$

where

$$|V_R(\bar{\nu})| = A_R\left[\frac{I_0(\bar{\nu})}{f_0(\bar{\nu})}\right] \exp[-a_R(\bar{\nu})l_R] \tag{11a}$$

and

$$\theta_R(\bar{\nu}) = \frac{\pi}{2} - a_R(\bar{\nu})l_R \tag{11b}$$

$$V(\omega_0, \beta_s) \approx \frac{pI_0}{2k\epsilon_0}\frac{\beta_s\eta_s}{k_s\sigma_p(\beta_s^2 - \sigma_s^2)}$$

$$\times \frac{2(r_s + b_{gs}) - [r_s + 1)(b_{gs} + 1)\exp(\sigma_s l_s) + (r_s - 1)(1 - b_{gs})\exp(-\sigma_s l_s)]e^{-\beta_s l_s}}{(b_{gs} + 1)(b_{ps} + 1)\exp(\sigma_s l_s) - (b_{gs} - 1)(b_{ps} - 1)\exp(-\sigma_s l_s)}. \tag{1}$$

with

$$A_R \equiv \frac{p(\alpha_R\alpha_p)^{1/2}}{2\pi(k\epsilon_0)k_R(b_{pR}+1)} \tag{12}$$

as the frequency-independent term.

Similarly, Eq. 8 may be adapted as follows:

$$V_{R_0}(f_0) = |V_{R_0}(\bar{\nu})|e^{i\theta_{R_0}} \tag{13}$$

with

$$|V_{R_0}(\bar{\nu})| = A_{R_0}\left[\frac{I_0(\bar{\nu})}{f_0(\bar{\nu})}\right] \tag{14a}$$

and

$$\theta_{R_0} = \frac{\pi}{2}; \qquad A_{R_0} \equiv \frac{p\alpha_p}{4\pi(k\epsilon_0)k_R}. \tag{14b}$$

Thermally Thick Sample. In this limit, pertinent to large thickness solids, one can set

$$l_s \gg \mu_s(f_0)\Big|_{\max} \tag{15}$$

where condition 15 must hold at the lowest modulation frequency, $f_0(\bar{\nu}_{\min})$, according to Eq. 9, i.e., for the maximum thermal diffusion length in the sample. Then $\exp(-\sigma_s l_s) \approx 0$ at all wavenumbers and Eq. 1 becomes:

$$V(\omega_0, \beta_s) \approx -\frac{pI_0}{2k\epsilon_0}\left[\frac{\beta_s\eta_s e^{-\beta_s l_s}}{k_s\sigma_p(\beta_s^2 - \sigma_s^2)}\right]\left(\frac{r_s+1}{b_{ps}+1}\right) \tag{16}$$

which may be divided by the blackbody reference, Eq. 13, to yield the spectrally normalized P²ES complex signal in the thermally thick limit:

$$S_N(\bar{\nu}) = C_s T(\bar{\nu})(\beta_s\mu_s)\left[\frac{2+(1-i)\beta_s\mu_s}{(\beta_s\mu_s)^2 - 2i}\right] \tag{17}$$

where

$$C_s \equiv \frac{(1+i)\eta_s(k_p\alpha_s^{1/2}/k_s\alpha_p^{1/2})}{2(b_{ps}+1)} \tag{18}$$

is a modulation frequency-independent factor, and

$$T(\bar{\nu}) \equiv e^{-\beta_s l_s} \tag{19}$$

is a transmittance factor, dependent on optical frequency through $\beta_s(\bar{\nu})$, but also independent of modulation frequency. Equation 17 is obtained when the experimental FT-IR-P²E spectrum of a thick sample is normalized by that of the PVDF detector covered only with a black infrared absorber whose thickness is very small compared to the shortest diffusion length, $\mu_{\min}$, a quantity which varies throughout an interferometer scan according to

$$\mu_s(\bar{\nu}) = \left(\frac{\alpha_s}{2\pi\nu\bar{\nu}}\right)^{1/2}. \tag{20}$$

Due to this variation with $\bar{\nu}$, FT-IR-P²E spectra, which are expected to resemble optical transmission spectra in the thermally thick limit,[20] will exhibit distortions with respect to the position and the height of sample absorption peaks, even after proper normalization. In order to account for such artifacts inherent in the thermal nature of the technique, a correction method, akin to the one applied by Teng and Royce[26] to FT-IR-PAS data, may be devised. Upon defining

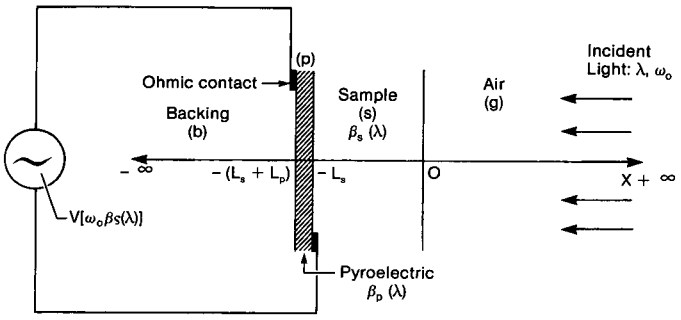

FIG. 1. One-dimensional geometry of a photopyroelectric system.

$$x \equiv \beta_s\mu_s \tag{21}$$

we may separate out Eq. 17 in real and imaginary components using:

$$S_N(\bar{\nu}) = C_s T(\bar{\nu})\left(\frac{x}{x^4+4}\right)Q(x) \tag{22}$$

where

$$Q(x) \equiv (x + 2 - ix)(x^2 + 2i). \tag{23}$$

Taking the magnitude of $Q(x)$ as $|Q(x)| = \sqrt{Q(x)Q^*(x)}$ and using the algebraic identity

$$x^4 + 4 \equiv (x^2 + 2x + 2)(x^2 - 2x + 2) \tag{24}$$

yields the following expression for the normalized FT-IR-P²ES amplitude:

$$|S_N(\bar{\nu})| = \sqrt{2}\,|C_s|\,T(\bar{\nu})\left[\frac{x}{\sqrt{x^2 - 2x + 2}}\right]. \tag{25}$$

Noting that $x = x(v, \nu)$, ratioing of two FT-IR-P²E spectra obtained at different scanning velocities ν_1 and ν_2 (say $\nu_2 > \nu_1$) and properly normalized, each by the appropriate blackbody spectrum *obtained at the same velocity*, gives the desired correction factor:

$$\frac{|S_N(\bar{\nu};\nu_1)|}{|S_N(\bar{\nu};\nu_2|} \equiv q(\bar{\nu}) = \left(\frac{x_1^2 - 2Rx_1 + 2R^2}{x_1^2 - 2x_1 + 2}\right)^{1/2}. \tag{26}$$

In Eq. 26 the ratio $q(\bar{\nu})$ is seen to be independent of $|C_s|$ and $T(\bar{\nu})$, as these factors are both independent of modulation frequency and cancel out of two spectral scans of the same sample. Futhermore,

$$x_1 \equiv x(\bar{\nu}, \nu_1) \tag{27}$$

$$R \equiv \left(\frac{\nu_2}{\nu_1}\right)^{1/2} \tag{28}$$

and, from the defining Eq. 21 and Eq. 20:

$$x_2 \equiv x(\bar{\nu}, \nu_2) = \frac{x_1}{R}. \tag{29}$$

Equation 26 establishes limiting values for $q(\bar{\nu})$ as follows: the optically opaque limit

$$x_1 \equiv \beta_s(\bar{\nu})\mu_s(\nu_1) \gg 1 \rightarrow q(\bar{\nu}) \approx 1, \tag{30}$$

and the optically transparent limit

$$x_1 \ll 1 \rightarrow q(\bar{\nu}) \approx R. \tag{31}$$

Experimentally, the function $q(\bar{\nu})$ may be obtained point-by-point throughout the two interferometer scans, at ν_1 and ν_2, while R can be calculated from Eq. 28. Solving the quadratic Eq. 26 for x_1 and keeping the positive root only, so that $x_1 > 0$ always, it can be shown that

$$x_1 = \frac{[q^2 - R + \sqrt{(R - q^2)^2 + 2(q^2 - 1)(R^2 - q^2)}]}{(q^2 - 1)} \equiv F(\bar{\nu}) \tag{32}$$

$$1 < q(\bar{\nu}) < R\,.$$

Equations 21 and 32 may now be used, in principle, to give absolute values for the optical absorption coefficient (i.e., corrected peak positions and heights) at all points (j) throughout the IR spectrum of a sample where data were collected, provided that the thermal diffusivity of the sample is accurately known:

$$\beta_s(\bar{\nu}_j) = \left(\frac{2\pi\nu_1}{\alpha_s}\right)^{1/2} \sqrt{\bar{\nu}_j}\, F(\bar{\nu}_j)\ [\mathrm{cm}^{-1}]. \tag{33}$$

In practice, it was found that FT-IR-P^{2}ES SNRs do not allow a very accurate calculation of the absolute absorption spectrum with the use of Eq. 33. Introduction of Eq. 32, however, into Eq. 25, as a correction factor, has been shown to yield high-quality relative absorption spectra corrected for source throughput and thermal diffusion length variation effects. Teng and Royce[26] have had similar success in obtaining corrected spectra using appropriate normalization techniques with FT-IR-PAS of thermally thick poly(methyl methacrylate) (PMMA) samples.

Thermally Thin Sample. This is a very important limit for FT-IR-P^{2}ES detection, as PVDF detectors have been shown to be quite sensitive to the presence of thin layers directly deposited on the electroded film surface.[27] The condition is

$$l_s \ll \mu_s(f_o)\Big|_{\min} \tag{34}$$

which must be satisfied for the highest modulation frequency, $f_0(\bar{\nu}_{\max})$, according to Eq. 9. Then $\exp(\pm\sigma_s l_s) \approx 1$ across the entire spectrum, and Eq. 1 becomes:

$$V(\omega_0, \beta_s) \approx \frac{pI_0}{2k\epsilon_0}\left[\frac{\beta_s\eta_s(1 - e^{-\beta_s l_s})}{k_s\sigma_p(\beta_s^2 - \sigma_s^2)}\right]\left(\frac{r_s + b_{gs}}{b_{ps} + b_{gs}}\right). \tag{35}$$

A procedure similar to the thermally thick case above yields the spectrally normalized P^{2}ES complex signal in the thermally thin limit:

$$S_N(\bar{\nu}) = C'_s A(\bar{\nu})(\beta_s\mu_s)\left[\frac{2b_{gs} + (1 - i)\beta_s\mu_s}{(\beta_s\mu_s)^2 - 2i}\right] \tag{36}$$

where

$$C'_s \equiv \frac{(1 + i)\eta_s(k_p\alpha_s^{1/2}/k_s\alpha_p^{1/2})}{2(b_{ps} + b_{gs})}, \tag{37}$$

and

$$A(\bar{\nu}) \equiv 1 - e^{-\beta_s l_s} \approx \beta_s l_s \tag{38}$$

is an absorptance factor, generating P^{2}E signals resembling absorption spectra in the thermally thin limit.[20] With the use of definition 21, Eq. 36 becomes:

$$S_N(\bar{\nu} = C'_s A(\bar{\nu})\left(\frac{x}{x^4 + 4}\right)Q'(x) \tag{39}$$

where

$$Q'(x) \equiv (x + 2b_{gs} - ix)(x^2 + 2i) \tag{40}$$

so that

$$|S_N(\bar{\nu})| = \sqrt{2}\,|C'_s|A(\bar{\nu})x\left[\frac{x^2 + 2b_{gs}x + 2b_{gs}^2}{x^4 + 4}\right]^{1/2}. \tag{41}$$

In view of Eq. 40, a sixth-order algebraic equation obtains for x_1 in terms of $q(\bar{\nu})$:

$$(q^2 - 1)x_1^6 + 2b_{gs}(q^2R - 1)x_1^5 + 2b_{gs}^2(q^2R^2 - 1)x_1^4 - 4(R^4 - q^2)x_1^2 - 8b_{gs}R(R^3 - q^2)x_1 - 8b_{gs}^2R^2(R^2 - q^2) = 0. \tag{42}$$

In the special case where the gas/sample interface thermal coupling coefficient $b_{gs} = 1$, Eq. 41 may be separated into the product of a quadratic and a quartic polynomial, the former of which is Eq. 26, giving the solution in Eq. 32, as expected from inspection of the forms of Eqs. 22 and 39. For all values of b_{gs}, however, the range of $q(\bar{\nu})$ values of Eq. 41 is, in this case too, $1 < q(\bar{\nu}) < R$.

Equation 42 requires numerical solution. In order to identify relatively simple limits for quantitative spectroscopic analysis, two cases of special interest may be considered in terms of the relative importance of b_{gs} in the entire range of $\beta_s(\bar{\nu})$ values. In Eq. 39, upon setting

$$x \gg 2b_{gs}\ [\text{i.e., } \beta_s(\bar{\nu}) \gg 2b_{gs}/(\mu_s)_{\min}] \tag{43}$$

and making the approximation $\mu_s(f_0) \approx \mu_{PVDF}(f_0)$—a reasonable assumption for very thin layers deposited directly on the pyroelectric detector—one arrives at the photothermally thick condition

$$\beta_s(\bar{\nu}) \gg 47\ \mathrm{cm}^{-1}. \tag{44}$$

Condition 44 was estimated with the use of the air-PVDF system, with[22] $\alpha_{PVDF} = 5.4 \times 10^{-4}$ cm^2/s, $k_{PVDF} = 0.13$ W/mK, and[28] $\alpha_{Air} = 0.19$ cm^2/s, $k_{Air} = 2.38 \times 10^{-2}$ W/mK; $b_{Air\text{-}PVDF} = 9.76 \times 10^{-3}$, $\mu_{PVDF}(1\ \mathrm{kHz}) = 4.15\ \mu$m. For materials with IR absorption coefficients satisfying Eq. 44, we may set $b_{gs} = 0$ in Eq. 41 and obtain:

$$x_1 = \sqrt{2}\left(\frac{R^4 - q^2}{q^2 - 1}\right)^{1/4} \equiv G(\bar{\nu}). \tag{45}$$

For discrete data points throughout the IR spectrum, Eq. 45 yields the corrected spectrum

$$\beta_s(\bar{\nu}_j) = \left(\frac{2\pi\nu_1}{\alpha_s}\right)^{1/2} \sqrt{\bar{\nu}_j}\, G(\bar{\nu}_j)\ [\mathrm{cm}^{-1}] \tag{46}$$

subject to relation 44.

In the opposite limit

$$x \ll 2b_{gs} \text{ [i.e., } \beta_s(\bar{\nu}) \ll 47 \text{ cm}^{-1}\text{]} \tag{47}$$

the same procedure yields

$$x_1 = \sqrt{2R}\left(\frac{R^2 - q^2}{q^2R^2 - 1}\right)^{1/4} \equiv H(\bar{\nu}) \tag{48}$$

with an analogous expression to Eq. 46 for the corrected spectrum:

$$\beta_s(\bar{\nu}_j) = \left(\frac{2\pi\nu_1}{\alpha_s}\right)^{1/2} \sqrt{\bar{\nu}_j} H(\bar{\nu}_j) \text{ [cm}^{-1}\text{]} \tag{49}$$

subject to relation 47. For very thin deposited films, the weighed thermal response over one modulation cycle is such that the composite thermal diffusion length of the (sample + PVDF) will be dominated by the much thicker PVDF. In this situation fairly accurate values for $\beta_s(\bar{\nu})$ should be obtained, in principle, by replacing α_s by α_{PVDF} in Eqs. 46 and 49.

EXPERIMENTAL AND RESULTS

The Bomem DA3 FT-IR spectrometer was used to obtain data throughout this work. This particular instrument has selectable mirror velocities—an important advantage over single-speed spectrometers, as it allows modulation frequency control and spectral corrections for the spectrally variable thermal diffusion length, as discussed in the previous section. Furthermore, the DA3 provides access to the interferogram phase, an important information and correction channel[29] in photothermal (and, in particular, in P²E)[19] spectroscopy. A Globar® source and a Ge-coated KBr beamsplitter provided optical interferograms in the 400–4000 cm^{-1} range; however, for these experiments the 800–4000 cm^{-1} span was chosen, as the spectral intensity diminished significantly below 800 cm^{-1}, as shown in Fig. 2A, representing the source throughput. This factor tended to generate unacceptable noise levels in the pyroelectric detector, which rendered the spectroscopic data below 800 cm^{-1} essentially irreproducible, especially those from weak absorbers. Thin (28 μm) Kynar® PVDF films from Pennwalt[22] were inserted in an Inficon® microbalance housing as described elsewhere.[30] The cell was mounted directly inside the sample chamber of the spectrometer with the use of existing optics and a mechanical spacer for fixing it to the chamber floor at approximately the focal plane of the Globar beam. Since there is no closure requirement for P²ES, the chamber could be purged *in situ* before any measurements were performed. The output voltage due to the photopyroelectric effect was carried outside the chamber by a coax cable via a Microdot-to-BNC connector. An Ithaco Model 1201 low-noise, wide-bandwidth preamplifier was then used to amplify the signals to a level compatible with the analog-to-digital converter (ADC) of the DA3 (~0.1–10 V). The output of the preamp was connected directly to the input board of the spectrometer, thus completing the FT-IR-P²ES circuit. Signal processing and analysis was carried out by standard

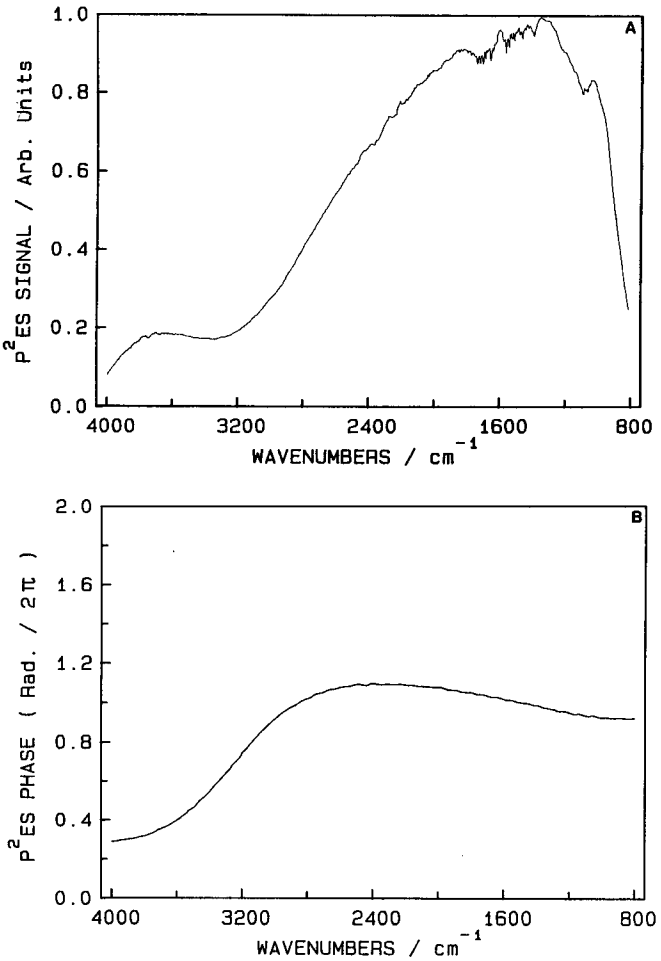

FIG. 2. FT-IR-P²E spectrum of Darco G-60 activated charcoal. Scanning speed: 0.02 cm/s; resolution: 2 cm^{-1}; preamplifier gain: 1000; coadded spectra: 30. **(A)** Amplitude; **(B)** phase.

Bomem software, modified to allow for quantitative manipulation of the spectra. Figure 2 shows the FT-IR-P²E spectrum of an ultra-thin layer (~1 μm) of activated charcoal (Spruce wood Darco G-60 from Fluka AG Buchs) on the surface of the Ni-Al ground electrode (350 nm) of the PVDF detector. The charcoal was dissolved in a mixture of solvents (2×10^{-2} M hexadecyl/trioxyethylene/Na_2SO_4, a surfactant from Henkel, and 30% EtOH from Fluka) and was placed on the detector in the form of a drop. Spectra were taken immediately after evaporation of the solvents following purging of the sample compartment with dry N_2. It may be observed from Fig. 2 that the usually-hard-to-eliminate, strongly interfering atmospheric CO_2 and H_2O absorptions present with other photothermal detection schemes (e.g., with PAS)[13] are essentially absent. Spectra were also obtained with the PVDF film as the sample and detector. The activated charcoal spectrum was then ratioed by the naked electroded PVDF spectrum. The results, shown in Fig. 3, indicate that there are essentially no spectral features due to the Ni-Al layered electrode. The much lower signals (factor of 8) obtained with the naked electroded PVDF can be understood in terms of the enhanced reflectivity of the metal compared to that of carbon. Due to the essential flatness of the ratio in Fig. 3, most subsequent spectra were normalized by the appropriate

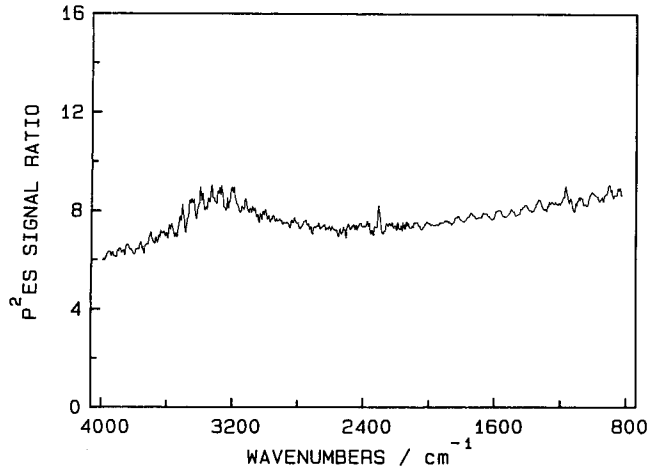

FIG. 3. Ratio of activated carbon and naked PVDF FT-IR-P²E spectra. Scanning speed: 0.02 cm/s; resolution: 2 cm⁻¹; preamplifier gain: 200; coadded spectra: 30.

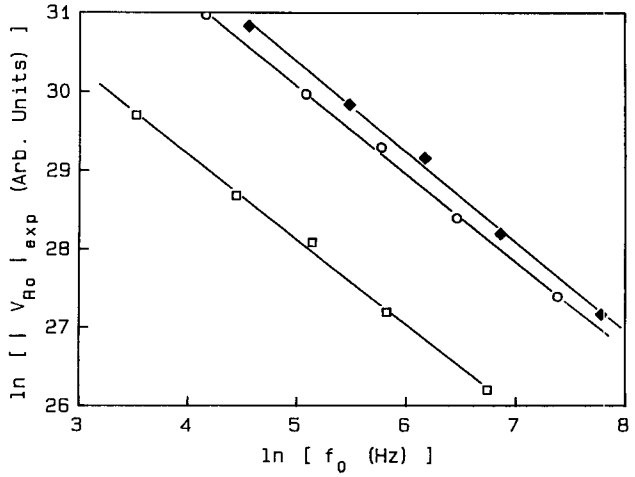

FIG. 4. Experimental relationship between FT-IR-P²E amplitude and mirror scanning velocity for a thin layer of black absorber at three wavenumbers. (□-□-□) 850 cm⁻¹; (○-○-○) 1600 cm⁻¹; (◆-◆-◆) 2400 cm⁻¹.

PVDF spectrum for experimental convenience. Implicit in the normalization process is the assumption that the normalizing spectrum is a faithful representation of the optical source photon flux within spectral bandwidths determined by the resolution. In the case of a thin black absorber layer on PVDF, one may write:

$$I_0(\bar{\nu}) = N(\bar{\nu})hc\bar{\nu} \tag{50}$$

where $N(\bar{\nu})$ is the photon flux at $\bar{\nu}$, and c is the speed of light. Inserting Eq. 50 in Eq. 14a and taking Eq. 9 into account yields

$$|V_{R_0}(\bar{\nu})| = A_{R_0}N(\bar{\nu})\left(\frac{hc}{2\nu}\right). \tag{51}$$

Equation 50 indicates that the P²E spectrum of Fig. 2 is independent of modulation frequency and scales with the source wavenumber variation only. On the other hand, at a fixed $\bar{\nu}$, the spectral magnitude should decrease as ν^{-1}. Figure 4 shows FT-IR-P²E spectral magnitude curves as functions of $f_0 = 2\bar{\nu}_0\nu$ at three widely different wavenumbers. The slopes of the least-squares fitted ln–ln plots were found to be -1.08 ($\bar{\nu}_0 = 850$ cm^{-1}), -1.11 ($\bar{\nu}_0 = 1600$ cm^{-1}), and -1.14 ($\bar{\nu}_0 = 2400$ cm^{-1}), thus indicating a $|V_{R_0}(\nu)|_{\text{exp}} \propto \nu^{-1.1}$ dependence, in good agreement with Eq. 51. For comparison, Fig. 5 shows similar curves obtained from the response of the pyroelectric DTGS detector accessory of the DA3 interferometer. In principle, the pyroelectric signals obtained by direct optical excitation of this detector should be similar to those obtained with PVDF. Figure 5 indicates, however, that the DTGS element does not behave ideally and may not be used for quantitative analyses. Complicating matters further, the DTGS detector is factory-covered with a polyethylene window as a spectral filter, which has sharp spectral features in the range of interest and which makes it ineligible as a P²E spectroscopic reference.

Much controversy exists as to the suitability of carbon black as a normalizing reference.[31,32] The non-flat spectral features of various types of carbon in the mid-IR cannot represent, in principle, the photon throughput of the source, a fact which has prompted Low and Parodi to advise against the use of carbon as a spectrum compensation source.[31] This problem does not appear to be critical with FT-IR-P²ES, as Fig. 3 shows that the activated carbon spectrum yields approximately a horizontal line when ratioed against the PVDF detector spectrum. This is an indication that the reflectance of the Ni-Al layered electrode does not contain sharp features in the 800–4000 cm^{-1} range, nor does the reflectance of the carbon overlayer; i.e., the spectrum of Fig. 2A is an essentially faithful representation of the photon flux per wavenumber of the Globar source. An advantage of FT-IR-P²E spectroscopy over the other photothermal techniques is in the use of the electroded PVDF spectrum (naked or carbon coated) as a normalizing source for transparent thick films and general thin film layers, where transmission type P²E spectra are expected: the spectral intensity registered with the detector at all wavelengths may be compensated *exactly* by the electroded PVDF spectrum, due to the fact that the detector acts as its own blackbody compensator and the result is free of any artifacts which may be present when the blackbody reflectance is different from that of the sample holder used during the experiment. This is indeed the case with FT-IR micro-

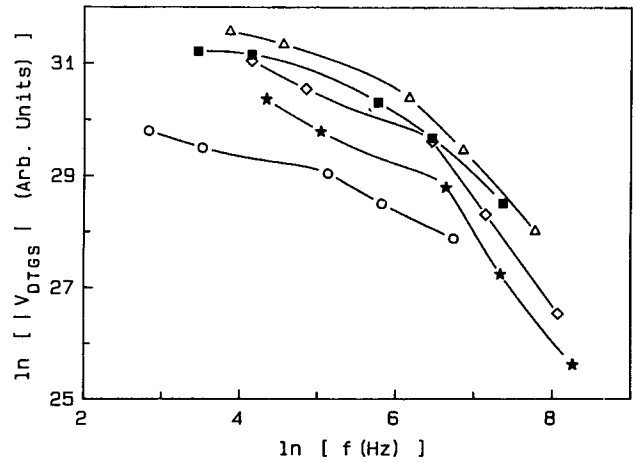

FIG. 5. The response of the Bomen DA3 DTGS pyroelectric detector as a function of mirror scanning velocity. (○-○-○) 850 cm⁻¹; (★-★-★) 3850 cm⁻¹; (◇-◇-◇) 3200 cm⁻¹; (◆-◆-◆) 1600 cm⁻¹; (△-△-△) 2400 cm⁻¹).

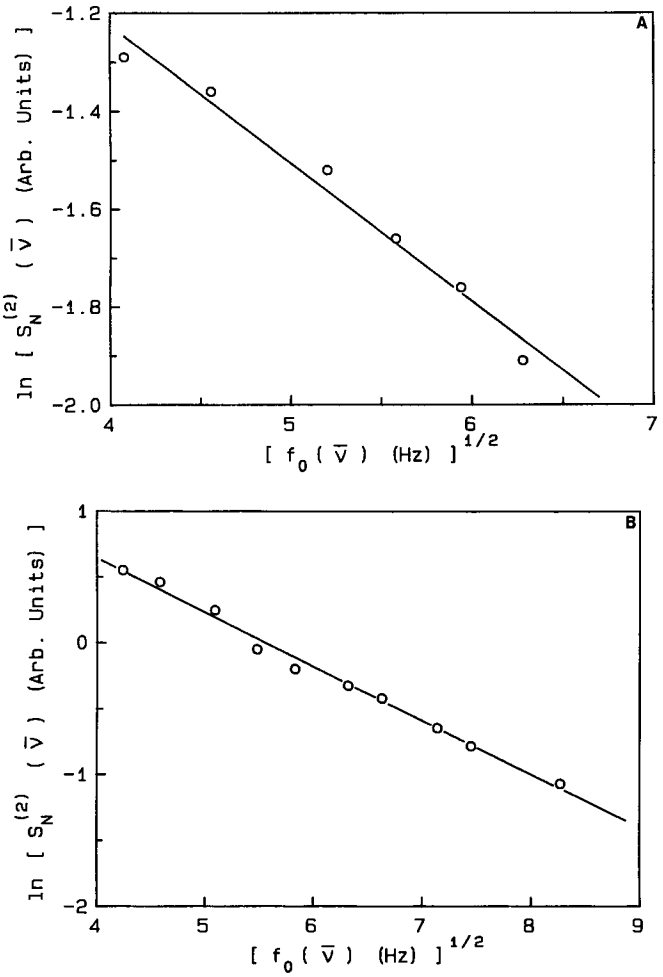

FIG. 6. FT-IR-P²E response of composite activated carbon-Mylar system. (**A**) $l_1^c = 13 \pm 2$ μm, $l_1^M = 20 \pm 2$ μm; (**B**) $l_2^c = 16 \pm 2$ μm, $l_2^M = 40 \pm 3$ μm. The abscissa is given in frequency units during an entire spectral scan from 800 to 4000 cm^{-1} with $f_0(\bar{\nu}) = 2v\bar{\nu}$ with $v = 0.01$ cm/s; resolution: 2 cm^{-1}; coaddition of 15 spectra.

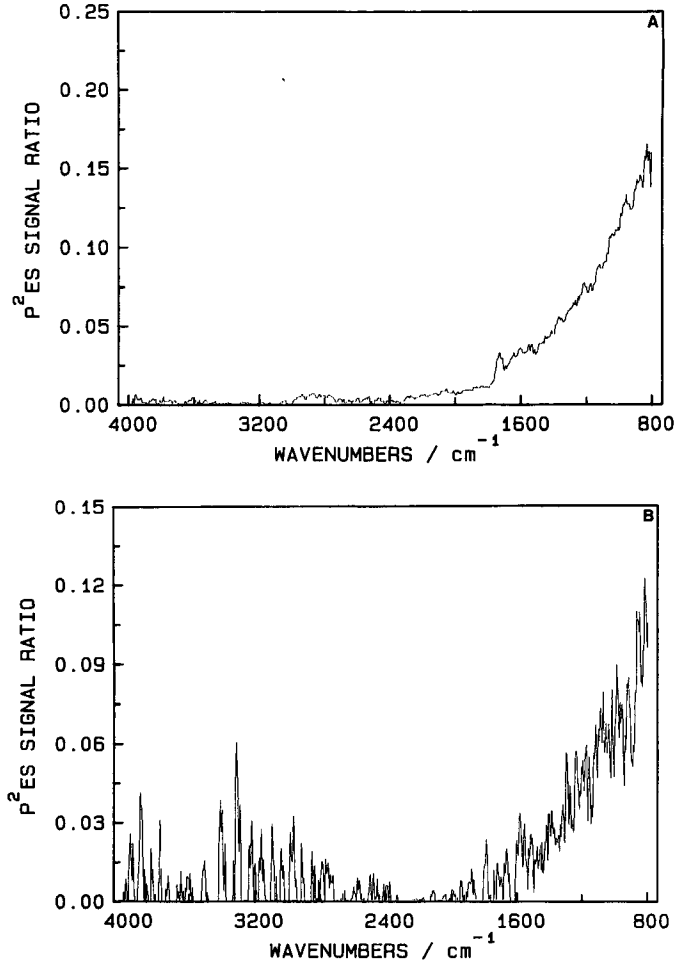

FIG. 7. FT-IR-P²E response to activated carbon-coated biomer, exhibiting the expected exponential decay with increasing wavenumbers (i.e., modulation frequency). Scanning speed: 0.01 cm/s; resolution: 2 cm^{-1}; coadded spectra: 20. (**A**) DA3 detector/preamplifier delay time = 1.6 ms; (**B**) 80 μs.

phonic photoacoustic and photothermal deflection spectroscopies and with any scheme which requires that the normalizing black absorber be removed from the detector after acquisition of the normalizing spectrum. The difficulties with this operation are nicely exemplified in the work by Riseman and Eyring.[32] The aforementioned advantage of FT-IR-P²E detection, of course, ceases to exist when optically opaque and thermally thin spectroscopy[23] is performed, since the optical characteristics of the detector become unimportant.

The effects of changing thermal diffusion length in a sample throughout an IR spectral scan were investigated with the use of Mylar coated with a black absorber, carbon black, as a surface thermal source, in direct contact with the PVDF detector. Combining Eqs. 11a and 14a yields for the normalized signal:

$$S_N \equiv \frac{|V_R(\bar{\nu})|}{|V_{R_0}(\bar{\nu})|} = \left(\frac{A_R}{A_{R_0}}\right)\exp\left[-\left\{\frac{\pi f_0(\nu)}{\alpha_R}\right\}^{1/2} l_R\right]. \quad (52)$$

For the purposes of this experiment, the finite thickness of the activated carbon had to be taken into account. Quantitatively, this is most conveniently done by extending Eq. 52 to a two-body system in a manner similar to the one presented by John *et al.* for visible dispersive P²ES in the thermally thick limit:[24]

$$S_N^{(2)} = \text{Const.} \times \exp\left\{-\sqrt{\pi}\left[\left(\frac{l^c}{\alpha_c^{1/2}}\right) + \left(\frac{l^M}{\alpha_M^{1/2}}\right)\right]\sqrt{f_0(\bar{\nu})}\right\} \quad (53)$$

where $l^c(l^M)$ and $\alpha_c(\alpha_M)$ is the thickness and thermal diffusivity, respectively, of carbon (Mylar). Figure 6 shows plots of the $\ln[S_N^{(2)}]$ vs. $f_0^{1/2}$ for two different sets of carbon-Mylar thicknesses. A system of two equations with two unknown quantities, α_c and α_M, was set up with the use of the slopes of the least-squares-fitted straight lines in Fig. 6A and 6B as follows:

$$l_1^c x + l_1^M y = \frac{0.409}{\sqrt{\pi}} = 0.231 \quad (54a)$$

$$l_2^c x + l_2^M y = \frac{0.282}{\sqrt{\pi}} = 0.159 \quad (54b)$$

with

$$x \equiv \alpha_M^{-1/2}, \qquad y \equiv \alpha_c^{-1/2}. \quad (54c)$$

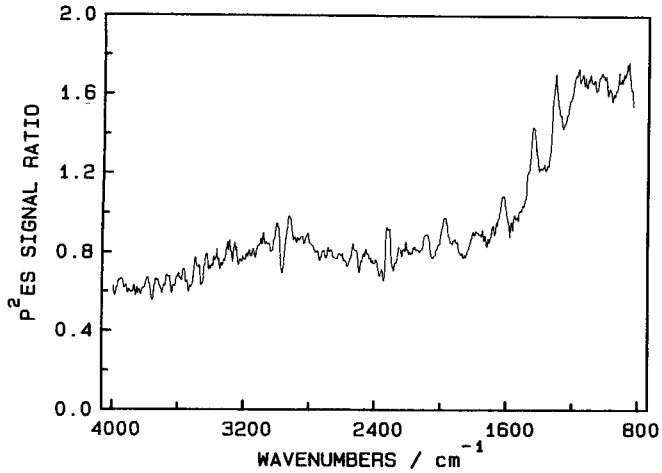

FIG. 8. FT-IR-P²E spectrum of silicone-based thermal compound deposited on the PVDF detector; preamplifier gain: 1000; v = 0.02 cm/s; resolution = 2 cm^{-1}; coadded spectra: 15.

Solution of Eqs. 54 yielded the values

$$\alpha_M = (1.9 \pm 0.5) \times 10^{-3}\ cm^2/s$$

and

$$\alpha_c = (2.6 \pm 1.0) \times 10^{-4}\ cm^2/s.$$

The experimental uncertainty values could be improved with a tighter control on our knowledge of the sample thicknesses, especially that of surface carbon. Our value for α_M compares well with the literature value deduced from data on polyethylene terephthalate (PETP Mylar) obtained by Angst and Pfister:[33]

$$\alpha_M = \frac{k_M}{\rho_M c_M} = \frac{0.26\ W/mK}{(1.37 \times 10^3\ kg/m^3) \times (1.09 \times 10^3\ J/kg\ K)} = 1.74 \times 10^{-3}\ cm^2/s.$$

No check on the α_c value could be made; however, the low value obtained is consistent with the experimentally observed large variations in the slope of the lines in Fig. 6 with small changes in the deposited carbon thickness.

An important instrumental feature of back-detection (FT-IR photothermal spectroscopy, such as FT-IR-P²ES, is the optimal setting of the detector/preamplifier delay command in the DA3 spectrometer. Due to the relatively slow thermal diffusion from surface absorbing layers to the position of the detector, it was found that optimal SNR could be obtained in all experimental cases if the time delay related to the 3 dB high cut-off frequency of the DA3 detector/preamplifier pair were set at the maximum available setting of 1.6 ms. This time constant is of the same order of magnitude as thermal transit times through many thin-layer media. The effect of the detector/preamplifier delay setting was minimal with thermally thin samples; however, considerable SNR improvement was observed with thick materials. As an example, Fig. 7 shows spectra of a carbon-coated biomer (used as a thermal delay medium), similar in nature to those of Fig. 6. The substantial enhancement of SNR with 1.5 ms delay compared with the 80-μs delay setting is evident from that figure. PVDF pyroelectric detector SNRs are generally subject to radiation noise, Johnson noise, and amplifier noise.[34] When the detector is used as a photopyroelectric sensor, the most ideal conditions exist when temperature fluctuation noise dominates. This gives the ideal area normalized detectivity limit.[35]

$$D^*_{ideal} = \frac{1}{4(k_B \sigma T^5)^{1/2}} = 1.8 \times 10^{10}\ cm\ Hz^{1/2}\ W^{-1}\ \text{at } 300\ K \quad (55)$$

where k_B is Boltzmann's constant, σ is Stefan's constant, and T is the absolute temperature. Real PVDF P²E detectors are usually limited by Johnson noise, and the detectivity is given by:[36]

$$D^*(\omega_0) = \frac{\eta l_p}{2(k_B T)^{1/2}} \left[\frac{p}{\rho_p C_p (k \epsilon_0 \tan \delta)^{1/2}} \right] \omega_0^{-1/2} \quad (56)$$

where $\rho_p C_p$ is the detector volume specific heat (=2.4 J cm^{-3} K), l_p is the detector thickness, η is the fraction of incident radiation absorbed ($\approx$1 for PVDF with carbon coating above the electroded surface), and tan δ is the dielectric dissipation factor (~0.01–0.02 in the range 1–10,000 Hz; Ref. 22, fig. 8). Phelan *et al.*[37] have measured the D^* for 1.86 cm^2 by 18-μm-thick PVDF. They have obtained values 1 × 10^8–2 × 10^6 cm $Hz^{1/2}$ W^{-1} for operation between 1 Hz and 1 kHz, respectively. These values are close to the highest available from other pyroelectric materials (e.g., TGS), and led to a material figure of merit (the quantity in brackets in Eq. 56) of 1.3 × 10^{-9} C cm J^{-1}.

In visible, dispersive P²ES it is often desirable to use a thermally bonding agent (e.g., No. 120-8 Wakefield thermal compound) between sample and PVDF detector to promote heat transfer to, and signal enhancement of, the PVDF detector.[38] This operation has no discernible effect in terms of introduction of artifacts to UV-VIS P²E spectra. In FT-IR-P²ES, however, care must be taken, as the spectrum of thermal compounds based on silicone (Fig. 8) exhibits substantial structure which could severely interfere with sample spectra obtained by this back-detection technique. Because of this effect, it was decided not to use thermally bonding compounds in FT-IR-P²ES in this work.

In order to evaluate the FT-IR spectroscopic capabilities of the technique, thermally thick and thin samples were used, in light of the theoretical discussion in the preceding section. The thick material was 125-μm Mylar directly in contact with the PVDF detector. With the use of α_m = 1.74 × 10^{-3} cm^2/s, the range of thermal diffusion lengths in the 800–4000 cm^{-1} region is found to be 41.6 μm $\geq \mu_M(f) \geq$ 18.6 μm at v = 0.02 cm/s and 26.3 μm $\geq \mu_M(f) \geq$ 11.8 μm at v = 0.05 cm/s. Therefore, the FT-IR-P²E spectrum of Mylar was thermally thick throughout the scanned spectral range and was expected to resemble an optical transmission spectrum (see Eq. 25). Figure 9A shows the spectral amplitude. Figure 9B is the transmission spectrum obtained from a Bomem Michelson 110 FT-IR spectrophotometer, with an MCT detector. It can be seen that the FT-IR-P²ES signal does resemble closely the transmission spectrum. In detail, however, there are a few differences between the two spectra. These differences concern the relative peak intensities, whereas peak (and valley) positions lie within the spectral resolution of each other (~4 cm^{-1}). The apparent spectral resolution exhibited by P²ES in the

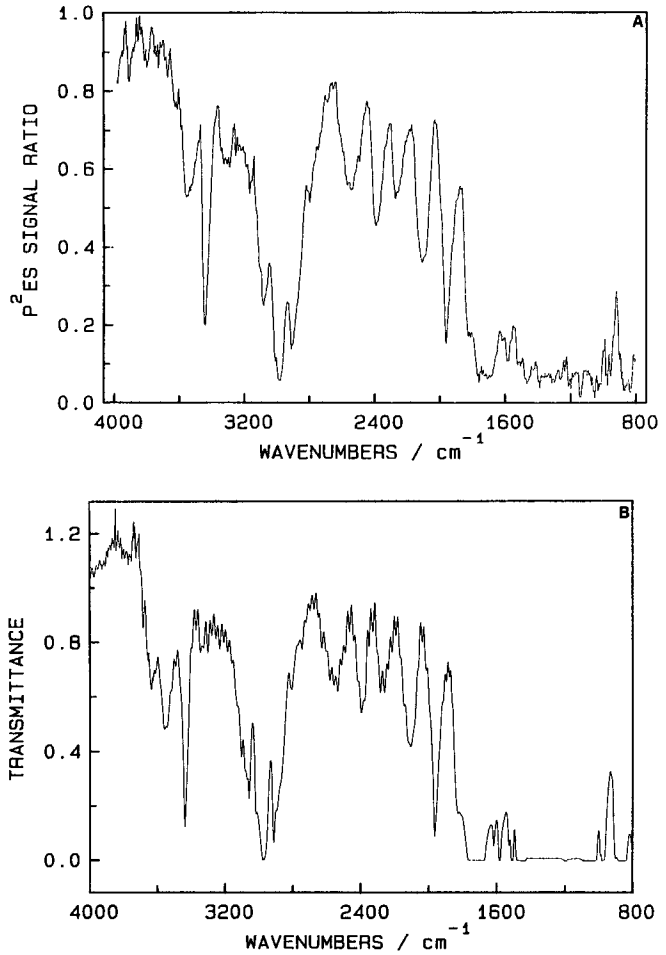

FIG. 9. (A) FT-IR-P²E spectrum of 125-μm Mylar sheet obtained at 0.05 cm/s; resolution: 2 cm^{-1}; preamplifier gain: 1000; coadded spectra: 30. (B) Optical transmission spectrum of the 125-μm Mylar sheet; resolution: 4 cm^{-1}; coadded spectra: 250.

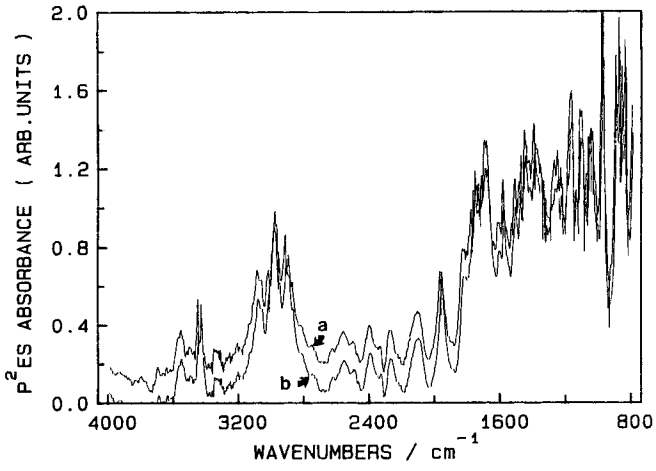

FIG. 10. FT-IR-P²E absorptance spectra of 125-μm Mylar sheet obtained at 0.02 cm/s; resolution: 2 cm^{-1}; preamplifier gain: 1000; coadded spectra: 30; (a) Corrected spectrum for thermal diffusion length contributions to P²E signal; (b) uncorrected spectrum.

optically opaque region below 1800 cm^{-1} (Fig. 9A), compared to several completely saturated regions of the optical transmission spectra (Fig. 9B), is well reproducible; however, the cause is not well understood. At this time it is speculated that the saturation threshold of the large-area PVDF transducer may be higher than that of the small-area MCT detector.

The P²ES Mylar absorbance was further calculated with the use of a spectrum similar to Fig. 9A, obtained at $\nu = 0.02$ cm/s, and standard DA3 Bomem software. The resulting spectrum is shown in Fig. 10 as spectrum **b**. Spectrum **a** in that figure is the result of the correction effected due to the thermal wave nature of FT-IR-P²ES, according to the theory presented earlier for thermally thick samples: The function $x_1 = F(\bar{\nu})$ was calculated according to Eq. 32 with $\nu_1 = 0.02$ cm/s and $\nu_2 = 0.05$ cm/s spectra of Mylar. Then the $x_1(\bar{\nu})$ spectrum was used in Eq. 25 as a compensation factor due to thermal diffusion length contributions to the signal, and Eq. 25 was then solved for $T(\bar{\nu})$ with the uncorrected normalized P²E spectrum as $|S_N(\bar{\nu})|$. Application of the same standard DA3 Bomem software then produced the corrected absorptance spectrum (**a**). Phenomenologically, the corrections produced an enhanced absorptance spectrum, except for regions of high $\beta_s(\bar{\nu})$, where the enhancement was small or null. Physically, the small but finite thermal contributions to the (otherwise purely) optical transmission P²E spectrum amounted to an effectively larger pyroelectric signal. FT-IR-P²E phase spectra of the Mylar sample also showed spectral structure mimicking the amplitude spectra of Fig. 9A and the one taken at 0.02 cm/s. This structure was superimposed on the instrumental baseline (Fig. 2B) and constitutes strong evidence of thermal transfer delays,[21] not expected from purely optical transmission through the body of the sample. The P²E signal was thus numerically interpreted as a smaller absorptance spectrum than that obtained with the use of optical transmittance spectra taken with the PVDF detector and the Mylar sample lying ~100 μm above the detector but not touching. The decreased (or absent) amount of correction at peaks in the 3430-cm^{-1}, 3000-cm^{-1}, 1960-cm^{-1}, and below 1000-cm^{-1} regions are associated with very strong absorptions, which appear in photopyroelectric saturation[21] in Fig. 10 and thus render the P²E spectra less sensitive (or insensitive) to variations in $\beta_s(\bar{\nu})$. This effect makes the right-hand side of Eq. 25 independent of x for $x \gg 1$. No significant shifts of the relative peak positions beyond the resolution bandwidths were found in the corrected Mylar spectrum of Fig. 10a, which implies that the uncorrected "raw" normalized spectrum (**b**) may be conveniently used for accurate qualitative peak identification in thermally thick solids, if quantitative absorption intensity profiles are not required.

As a thermally thin material we used Probimide® 408, a high-photospeed polyimide[39] utilized in the semiconductor industry as dielectric layers, alpha particle barriers in memory devices, ion implant masks, and passivation layers.[40] The polyimide was spun on the PVDF detector at 3300 rpm for 25 s so as to obtain a 1-μm-thick film, according to the CIBA-GEIGY processing instruction manual. Subsequently, FT-IR-P²E spectra were obtained with scanning speeds between 0.02 and 0.7 cm/s. It is worth mentioning that high SNRs at 0.7 cm/s allowed ready identification of sharp peaks below 2000 cm^{-1} with only 800 coadded spectra. The maximum speed was limited by the DA3 scanning capabilities. The FT-

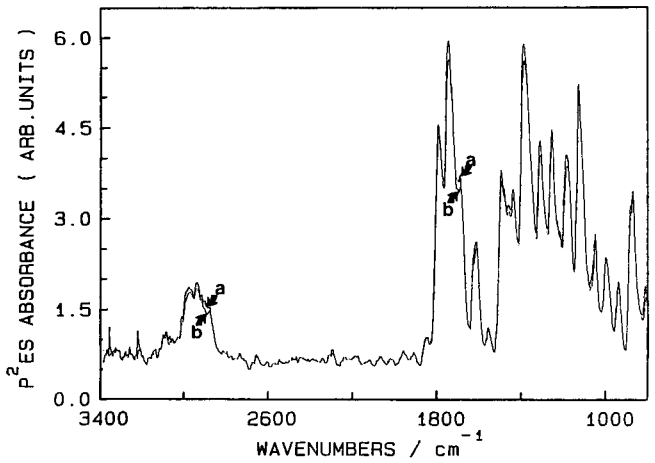

FIG. 11. FT-IR-P²E absorptance spectra of 1-μm Probimide® 408 obtained at 0.02 cm/s; resolution: 2 cm^{-1}; preamplifier gain: 1000; coadded spectra: 15; (a) Corrected spectrum for thermal diffusion length contributions to P²E signal; (b) uncorrected spectrum.

IR spectra thus obtained were found to be similar to optical absorption spectra characteristic of polyimides,[41] including the 1726- and 1776-cm^{-1} peaks due to carbonyl absorption. No independent IR absorption spectra of Probimide® itself were available for direct comparison. It is well-known that Probimide® is akin in molecular structure to Kapton® (H-Film; poly-4,4′-oxydiphenylene-pyromeltimide). Mid-IR spectra of that polymer have been recorded, by Wrasidlo,[42] exhibiting the characteristic amide-NH stretching vibrations in the 3000–3500 cm^{-1} range, in agreement with similar absorption features in the spectrum of Fig. 11. In order to ascertain whether there was a necessity for spectral corrections, due to the photothermal nature of our spectra, the function $x_1 = G(\bar{\nu})$ was calculated according to Eq. 45 with the $\nu_1 = 0.02$ cm/s and $\nu_2 = 0.1$ cm/s spectra of Probimide®. Equation 46 was then evaluated with $\alpha_s = \alpha_{PVDF}$, and the resulting absolute optical absorption coefficient values $\beta_s(\bar{\nu})$ were found to be consistent with assumption 44 throughout the experimental wavenumber range. Finally, Eq. 41 with the thin-film approximation (Eq. 38) and with $b_{gs} = b_{Air.PVDF} = 9.76 \times 10^{-3}$ was solved for $A(\bar{\nu})$ with the uncorrected normalized P²E spectrum at $\nu = 0.02$ cm/s as $|S_N(\bar{\nu})|$. The results are shown in Fig. 11 as spectrum **a**. Spectrum **b** is the "raw" normalized P²E spectrum. It can be seen that the corrected spectrum is very close to the uncorrected one, with a slight enhancement throughout the 800–3400 cm^{-1} range. It may be concluded that for all practical purposes the raw normalized spectrum of Probimide® suffices for quantitative spectroscopic studies. The near coincidence of the two spectra is a manifestation of the purely thermal nature of the P²E spectrum of the Probimide® film, which is entirely thermally thin at 1 μm thickness. The very high reproducibility of thin-film FT-IR-P²E spectra is, at least partially, associated with the blackbody normalization advantage of this technique, as discussed earlier. The spectrum of the Probimide® film on the PVDF detector was taken again after exposure of the film to ~360 nm radiation from a Xe lamp for 2 min. Although there was a visible change in the color of the film after the exposure associated with the interaction of the UV light with the polyamic acid polymer bearing photoreactive side groups,[40] no spectral changes were observed in the FT-IR-P²E spectrum. This is an indication that no significant breaking up of the polymer chains occurred during irradiation. A systematic study of the P²E spectrum as a function of irradiation history, without further destructive processing, may contribute useful insights into the photochemical processes occurring in the Probimide® molecular system.

CONCLUSIONS

In this work Fourier transform infrared photopyroelectric spectroscopy has been introduced as a new technique capable of experimentally convenient qualitative analysis and theoretically relatively simple quantitative calculation. It was found that an experimentally derived numerical correction is required for spectra obtained in the thermally thick limit. No such correction was found necessary for thermally thin spectra, although a comprehensive theoretical method for doing so was developed as part of a general theoretical framework for FT-IR-P²ES. The technique appears to be most promising in the study of thin layers deposited directly on PVDF, especially when used to monitor interactions with external agents *in situ*.

ACKNOWLEDGMENTS

The authors would like to acknowledge the valuable assistance of Dr. J. Moser for the preparation of the activated charcoal blackbody solution used in this work. Partial support of the Ontario Laser and Lightwave Research Center (OLLRC) is gratefully acknowledged. One of us (A. Mandelis) wishes to thank Professor E. Kovats for the invitation to EPFL during a sabbatical research leave.

1. P. R. Griffiths and J. A. de Haseth, *Fourier Transform Infrared Spectrometry* (Wiley-Interscience, New York, 1986), Chap. 9, pp. 312–337.
2. D. W. Vidrine, "Photoacoustic Fourier Transform Infrared Spectroscopy of Solids and Liquids," in *Fourier Transform Infrared Spectroscopy*, J. R. Ferraro and L. J. Basile, Eds. (Academic, New York, 1982), Vol. 3, Chap. 4, pp. 125–148.
3. B. S. H. Royce, "Fourier Transform Photoacoustic Spectroscopy of Solids," in *Photoacoustic and Thermal Wave Phenomena in Semiconductors*, A. Mandelis, Ed. (North-Holland, New York, 1987), Chap. 11, pp. 276–281.
4. S. A. Yeboah, S-H. Wang, and P. R. Griffiths, Appl. Spectrosc. **38,** 259 (1984).
5. G. Laufer, J. T. Huenke, B. S. H. Royce, and Y. C. Teng, Appl. Phys. Lett. **37,** 517 (1980).
6. S. M. Riseman, S. I. Yaniger, E. M. Eyring, D. A. MacInnes, A. G. MacDiarmid, and A. J. Heeger, Appl. Spectrosc. **35,** 557 (1981).
7. S. R. Lowry, D. G. Mead, and D. W. Vidrine, Anal. Chem. **54,** 546 (1982).
8. D. Débarre, A. C. Boccara, and D. Fournier, Appl. Opt. **20,** 4281 (1981).
9. M. J. D. Low, C. Morterra, and A. B. Severdia, Spectrosc. Lett. **15,** 415 (1982).
10. D. J. Gerson, J. F. McClelland, S. Veysey, and R. Markuszewski, Appl. Spectrosc. **38,** 902 (1984).
11. J. C. Donini and K. H. Michaelian, Infrared Phys. **24,** 157 (1984).
12. N. Teramae and S. Tanaka, Anal. Chem. **57,** 95 (1985).
13. L. B. Lloyd, R. C. Yeates, and E. M. Eyring, Anal. Chem. **54,** 549 (1982).
14. S. J. McGovern, B. S. H. Royce, and J. B. Benziger, J. Appl. Phys. **57,** 1710 (1985).
15. T. Hashimoto, J. Cao, and A. Takaku, Thermochim. Acta **120,** 191 (1987).
16. B. S. H. Royce, S. J. McGovern, and J. B. Benziger, American Laboratory, 1 (March 1985).

17. P. G. Varlashkin and M. J. D. Low, Infrared Phys. **26,** 171 (1986).
18. A. Mandelis, J. Appl. Phys. **54,** 3403 (1983).
19. H. Coufal, Appl. Phys. Lett. **44,** 59 (1984).
20. A. Mandelis, Chem. Phys. Lett. **108,** 388 (1984).
21. A. Mandelis and M. M. Zver, J. Appl. Phys. **57,** 4421 (1985).
22. *Kynar® Piezo Film Technical Manual* (Pennwalt Corporation, King of Prussia, Pennsylvania, 1983), p. 17.
23. A Rosencwaig and A. Gersho, J. Appl. Phys. **47,** 64 (1976).
24. P. K. John, L. C. M. Miranda, and A. C. Rastogi, Phys. Rev. B **34,** 4342 (1986).
25. P. R. Griffiths and J. A. de Haseth, *Fourier Transform Infrared Spectrometry* (Wiley-Interscience, New York, 1986), Chap. 1.
26. Y. C. Teng and B. S. H. Royce, Appl. Opt. **21,** 77 (1982).
27. H. Coufal and A. Mandelis, "Photopyroelectric Spectroscopy of Semiconductors," in *Photoacoustic and Thermal Wave Phenomena in Semiconductors,* A. Mandelis, Ed. (North-Holland, New York, 1987), Chap. 7, pp. 149–173.
28. A. Rosencwaig, *Photoacoustics and Photoacoustic Spectroscopy* (Wiley-Interscience, New York, 1980), p. 96.
29. M. Choquet, G. Rousset, and L. Bertrand, Can. J. Phys. **64,** 1081 (1986).
30. H. J. Coufal, R. K. Grygier, D. E. Horne, and J. E. Fromm, J. Vac. Sci. Technol. A **5,** 2875 (1987).
31. M. J. D. Low and G. A. Parodi, Spectrosc. Lett. **13,** 663 (1980).
32. S. M. Riseman and E. M. Eyring, Spectrosc. Lett. **14,** 163 (1981).
33. *Kunststoff-Information Katalog* (Angst and Pfister A.G., Zürich, Switzerland, 1988), p. 17.
34. R. W. Whatmore, Rep. Prog. Phys. **49,** 1335 (1986).
35. E. H. Putley, Infrared Phys. **20,** 149 (1980).
36. G. Burdick and R. T. Arnold, J. Appl. Phys. **37,** 3223 (1966).
37. R. J. Phelan, Jr., R. J. Mahler, and A. R. Cook, Appl. Phys. Lett. **19,** 337 (1971).
38. A. Mandelis, F. Care, K. K. Chan, and L. C. M. Miranda, Appl. Phys. A **38,** 117 (1985).
39. Manufactured by CIBA-GEIGY Ltd. Electronic Materials K-401.1.10, CH-4002 Basle, Switzerland.
40. O. Rohde, M. Riediker, A. Schaffner, and J. Bateman, Solid State Technol., Sept. (1986).
41. D. O. Hummel, *Atlas der Kunststoff-Analyse; Band I: Hochpolymere und Harze* (Carl Hanser Verlag, München, 1968), polymide spectra #1249–1255.
42. W. J. Wrasidlo, J. Polym. Sci., Polym. Phys. Ed. **11,** 2143 (1973).